https://doi.org/10.2352/ISSN.2470-1173.2017.13.IPAS-215


# Alpha-Rooting Method of Gray-scale Image Enhancement in The Quaternion Frequency Domain

Artyom M. Grigoryan and Sos S. Agaian

Department of Electrical and Computer Engineering
The University of Texas at San Antonio

## ABSTRACT

New models of gray-scale image representation in the 4-D quaternion space are described, wherein images can be processed as quaternion and color images in the frequency domain, by using the concepts of the 2-D quaternion unitary transforms, such as quaternion discrete Fourier transforms, wavelet, and others. Methods of alpha-rooting by such 2-D transforms can be effectively used for gray-scale image enhancement, and optimal parameters enhancements can be found by using the measures EME and EMEC, and image visibility measures of image enhancement. Different models of transferring the gray-scale images into the quaternion space can be applied, which include models $2 \times 2$, $4 \times 1$, $4 \times 1$, and others.

**Keywords:** Image enhancement, alpha-rooting, Fourier transform, discrete quaternion Fourier transform.

## 1. INTRODUCTION

The goal of image enhancement techniques is to improve a characteristic or quality of an image, such that the resulting image is better than the original, when compared against specific criteria. The digital image enhancement has remained one of the most active research areas in image processing and computer vision. Two major classifications of image enhancement techniques can be defined: spatial domain enhancement and transform domain enhancement. Transform-based methods of image enhancement are based on manipulation with all or part of spectral components of the transform. We focus on the well-known method of alpha-rooting, although other methods, including the log-alpha-rooting, modified unsharp masking, and methods based on wavelet transforms are also used in image enhancement. Many traditional methods of image enhancement were applied for processing the color images. In the last decade, the concept of the 2-D DFT was generalized and the 2-D quaternion discrete Fourier transforms (QDFT) were introduced and applied to color imaging[1]-.[4] The 2-D QDFT include the two-side, right-side, and left-side QDFTs.[5] These transforms are fast and there algorithms are based on representation of the QDFT by a combinations of a few classical DFT transforms.[6] This allows us to obtain 1-D and 2-D QDFT fast numerical implementation with the standard FFT algorithms.[11,14,21,22] These transforms can found effective applications in color imaging,[15,19] medical imaging[16]-,[18] in image filtration,[1,31] image enhancement[20,26]-.[30] The 2-D QDFT can be used not only in color imaging, but in gray-scale imaging as well, and for that there are many models of transferring one or a few gray-scale images to the quanterion space.[1]

In this paper, new methods of image enhancement are proposed for enhancement grays-scale images, which are based on constructing models and transferring the images to quaternion space, where images can be considered as 4-D quaternion with the 3-D color image component images. In the quaternion space, as well as in the color space, images can effectively be processed and then transformed back to the gray-scale images. The application of the concept of the two-dimension discrete quaternion Fourier transform (2-D QDFT) together with the methods of image enhancement and filtration results in high quality images, when comparing with traditional processing by the 2-D DFT. The methods of alpha-rooting, weighted alpha-rooting and other modification of alpha-rooting in the quaternion space allows to achieve new results in gray-scale imaging. The image enhancement technique of alpha rooting can be used for enhancing high contrast edge information and sharp features in images. Therefore the use of the 2-D DQFT in alpha-rooting adapted to the quaternion image representations is much promised. Our preliminary results show that the application of the 2-D QDFT plus alpha-rooting method can be effectively used for enhancing gray-scale images. Examples of application of the proposed method on different gray-scale images and comparison with the traditional method when the 2-D DFT based alpha-rooting are given. To estimate the quality of the gray-scale and color image enhancement, we used the known EME and EMEC measures of image enhancement and applied it for images enhanced by both 2-D QDFT and 2-D DFT.

## 2. BLOCK-DIAGRAM OF GRAY-SCALE IMAGING

The general block-diagram of gray-scale image processing in the quaternion space of frequencies is shown in Figure 1.

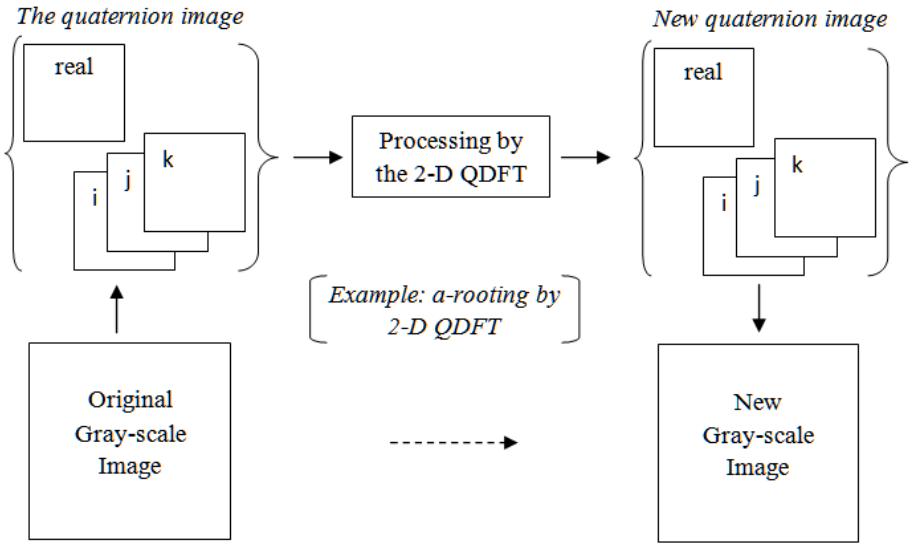


Figure 1. The block-diagram of gray-scale image processing in the frequency domain.

The processing is by the 2-D quaternion discrete Fourier transform (QDFT). In image enhancement, the methods of enhancement by the 2-D QDFT can be considered, including the method of $\alpha$-rooting,[13,20] which will be described in next sections.

This diagram describes the gray-scale image processing by the following steps.

Step 1. Gray scale image $f_{n,m}$ of size $N \times M$ is transformed into the quaternion image $q_{n,m}$

$$\{f_{n,m};\, n = 0 : (N-1),\, m = 0 : (M-1)\} \to \{q_{n,m};\, n = 0 : (N_1 - 1),\, m = 0 : (M_1 - 1)\},$$

The quaternion image has the size smaller than the original image, for instance $N_1 = N/2$ and $M_1 = M/2$ considering $N$ and $M$ even. Given pixel $(n, m)$, the value of the quaternion image at this pixel is a quaternion number written as

$$q_{n,m} = a_{n,m} + (i(q_i)_{n,m} + j(q_j)_{n,m} + k(q_k)_{n,m}),$$

where $i, j$, and $k$ are quaternion units, $i^2 = j^2 = k^2 = -1$. All numbers $a_{n,m}$, $(q_i)_{n,m}$, $(q_j)_{n,m}$, and $(q_k)_{n,m}$ are real.

Step 2. The quaternion image $q_{n,m}$ is processed in the frequency domain

$$q_{n,m} \to \hat{q}_{n,m}, \quad n = 0 : (N_1 - 1),\, m = 0 : (M_1 - 1),$$

by using the concept of the 2-D QDFT. Different methods of enhancement and filtration, including the alpha-rooting, can be used for processing the image. The concept of 2-D QDFT has different definitions, such as the right-side, left-side, two-side 2-D QDFT, and all of them can be used. Instead of the Fourier transform, the concept of the 2-D quaternion wavelet transform and other transforms can also be used.

Step 3. The processed quaternion image $\hat{q}_{n,m}$ is transformed back into gray-scale

$$\{\hat{q}_{n,m};\, n = 0 : (N_1 - 1),\, m = 0 : (M_1 - 1)\} \to \{\hat{f}_{n,m};\, n = 0 : (N-1),\, m = 0 : (M-1)\}.$$

The gray-scale image $\hat{f}_{n,m}$ is the new processed (enhanced or filtered) image. Thus, the gray-scale image processing $f_{n,m} \to \hat{f}_{n,m}$ is accomplished through the quaternion space.

## 3. QUATERNION AND IMAGES

The quaternion are four-dimensional generation of a complex number with one real part and three component imaginary part.[1,9,10] The imaginary dimensions are represented as $i, j$, and $k$. In practice, the $i, j$, and $k$ are orthogonal to each other and to the real numbers. Any quaternion $q$ may be represented in a hyper-complex form as

$$q = a + bi + cj + dk = a + (bi + cj + dk),$$

where $a, b, c$, and $d$ are real numbers and $i, j$, and $k$ are three imaginary units with multiplication laws: $ij = -ji = k$, $jk = -kj = i$, $ki = -ik = -j$, $i^2 = j^2 = k^2 = ijk = -1$. The table of multiplications of imaginary numbers $i, j, k$, and 1 is given in Table 1.

| | 1 | $i$ | $j$ | $k$ |
|---|---|---|---|---|
| 1 | 1 | $i$ | $j$ | $k$ |
| $i$ | $i$ | -1 | $k$ | -$j$ |
| $j$ | $j$ | -$k$ | -1 | $i$ |
| $k$ | $k$ | $j$ | -$i$ | -1 |

Table 1. The table of multiplications of the four quaternion unit numbers.

The number $a$ is considered to be the real part of $q$ and $(bi + cj + dk)$ is the "imaginary" part of $q$. The quaternion conjugate and modulus of $q$ equal $\bar{q} = a - (bi + cj + dk)$, and $|q| = \sqrt{a^2 + b^2 + c^2 + d^2}$, respectively. The property of commutativity does not hold in quaternion algebra, i.e., there are many quaternions $q_1 \neq q_2$, such that $q_1 q_2 \neq q_2 q_1$. Given pure unit quaternion $\mu$, the quaternion exponential function at angle $\psi$ is calculated by $e^{-\mu\psi} = \cos(\psi) - \mu \sin(\psi), \quad (\mu^2 = -1, |\mu| = 1)$. This function is used in the concept of the 1-D and 2-D quaternion discrete Fourier transform (QDFT). In many applications the simple cases of $\mu$ are considered, such as $\mu = j$ and $\mu = k$.

It is not difficult to transfer the color image from the RGB model to the quaternion space. The three components, R(ed), G(reen), and B(lue) of discrete color image $f_{n,m}$ at each pixel can be considered together as the imaginary part of the a quaternion image, $f_{n,m} = 0 + (r_{n,m} i + g_{n,m} j + b_{n,m} k)$.

## 4. GRAY-SCALE-TO-QUATERNION MODEL

In this section, we present the simple model of $(2 \times 2)$-mapping, which is described as follows. The gray-scale image $f_{n,m}$ of size $N \times M$ can be divided by four parts with even-even, even-odd, odd-even, and odd-odd indices

| . | . | . | . | . | . |
|---|---|---|---|---|---|
| . | $f_{2n,2m}$ | $f_{2n,2m+1}$ | $f_{2n,2m+2}$ | $f_{2n,2m+3}$ | . |
| . | $f_{2n+1,2m}$ | $f_{2n+1,2m+1}$ | $f_{2n+1,2m+2}$ | $f_{2n+1,2m+3}$ | . |
| . | $f_{2n+2,2m}$ | $f_{2n+2,2m+1}$ | $f_{2n+2,2m+2}$ | $f_{2n+2,2m+3}$ | . |
| . | $f_{2n+3,2m}$ | $f_{2n+3,2m+1}$ | $f_{2n+3,2m+2}$ | $f_{2n+3,2m+3}$ | . |
| . | . | . | . | . | . |

Table 2. Image as a table

as follows:

$$\begin{aligned} f_e &= \{(f_e)_{n,m}\} = \{f_{2n,2m}\}, \qquad f_i = \{(f_i)_{n,m}\} = \{f_{2n,2m+1}\}, \\ f_j &= \{(f_j)_{n,m}\} = \{f_{2n+1,2m}\}, \quad f_k = \{(f_k)_{n,m}\} = \{f_{2n+1,2m+1}\}, \end{aligned}$$

where $n = 0 : (N/2-1)$, $m = 0 : (M/2-1)$. It is assumed, that $N$ and $M$ are even, if not, the borders of indexes should be corrected. As an example, Figure 2 shows the gray-scale "pentagon" image $f_{n,m}$.

The four parts can be considered as components of the quaternion matrix which we call the quaternion image and denote by $q(f)$,

$$q(f) = (f_e, f_i, f_j, f_k) = f_e + (i f_i + j f_j + k f_k).$$

The first part, the matrix of size $N/2 \times M/2$ is denoted by $f_e$ as the $e$-component, or real component of $q(f)$. Other three parts can be considered as the components of the imaginary part of the quaternion image. Therefore,

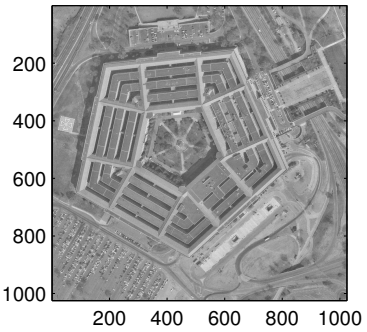


Figure 2. The gray-scale pepper image of size $1024 \times 1024$.

they can be denoted as $f_i$, $f_j$, and $f_k$ for the $i, j$, and $k$-components, respectively. Thus, when transforming the gray-scale image into the quaternion subspace, we may assume that the components $f_i$, $f_j$, and $f_k$ are the set-components of the imaginary part of the quaternion image, as shown in Table 3.

Mapping of the gray-scale image into the quaternion image

| | | | | | |
|---|---|---|---|---|---|
| . | . | . | . | . | . |
| . | **E**: $f_{2n,2m}$ | **R**: $f_{2n,2m+1}$ | **E**: $_{2n,2m+2}$ | **R**: $f_{2n,2m+3}$ | . |
| . | **G**: $f_{2n+1,2m}$ | **B**: $f_{2n+1,2m+1}$ | **G**: $f_{2n+1,2m+2}$ | **B**: $f_{2n+1,2m+3}$ | . |
| . | **E**: $f_{2n+2,2m}$ | **R**: $f_{2n+2,2m+1}$ | **E**: $f_{2n+2,2m+2}$ | **R**: $f_{2n+2,2m+3}$ | . |
| . | **G**: $f_{2n+3,2m}$ | **B**: $f_{2n+3,2m+1}$ | **G**: $f_{2n+3,2m+2}$ | **B**: $f_{2n+3,2m+3}$ | . |
| . | . | . | . | . | . |

Table 3. The gray-scale image mapping to the RGB color model.

Here, the letter **E** stands for the gray-levels, **R** for the red color, **G** for the green color, and **B** for the blue color. We assume that the component $f_i$ is set to the red color channel, and $f_j$ and $f_k$ to the green and blue channels, respectively, as shown in Table 3.

Figure 3 shows the real part $(f_e)_{n,m}$ in part a, and the components $(f_i)_{n,m}$, $(f_j)_{n,m}$, and $(f_k)_{n,m}$ in parts b, c, and d, respectively.

Thus, we obtain the full quaternion "pentagon" image with non-zero real part. The components of imaginary part can be mapped into one of the color spaces, such as the RGB or XYZ space.[1,2] In such a mapping, the imaginary part of the quaternion image $q(f)$ can be illustrated as a color image.

Figure 4 shows the real part $(f_e)_{n,m}$ of the quaternion image in part a and the imaginary part, or color image in b. These two images, namely the gray-scale image and color image of size $512 \times 512$ each, represent the original gray-scale "pentagon" image of size $1024 \times 1024$ in the quaternion space.

## 5. IMAGE ENHANCEMENT

After mapping the gray-scale image to the quaternion image, one can perform the 2-D quaternion transform-based method of image enhancement, which can be described by the block-diagram shown in Figure 5. The 2-D quaternion transform, such as for instance the right-side 2-D QDFT, is calculated over the quaternion image. Then the spectral coefficients $Q_(p, s)$ are manipulated as $Q_(p, s) \to C(p, s)Q_(p, s)$, $p, s = 0 : (N - 1)$. and the inverse transform is performed. Here, $C(p, s)$ is a function of coefficients of the 2-D QDFT. In the alpha-rooting image enhancement, the magnitude of the Fourier transform of the gray-scale image is transformed as[18,20]

$$|Q_(p, s)| \to M(|Q_(p, s)|) = |Q_(p, s)|^{\alpha}, \quad p, s = 0 : (N - 1).$$

for each sample $(p, s)$, and the parameter $\alpha$ is taken to be in the interval $(0, 1)$. Here $M$ is operator on magnitude of the transform, which is in alpha-rooting is the power function. The coefficients $C(p, s)$ equal $|Q_(p, s)|^{1-\alpha}$. The

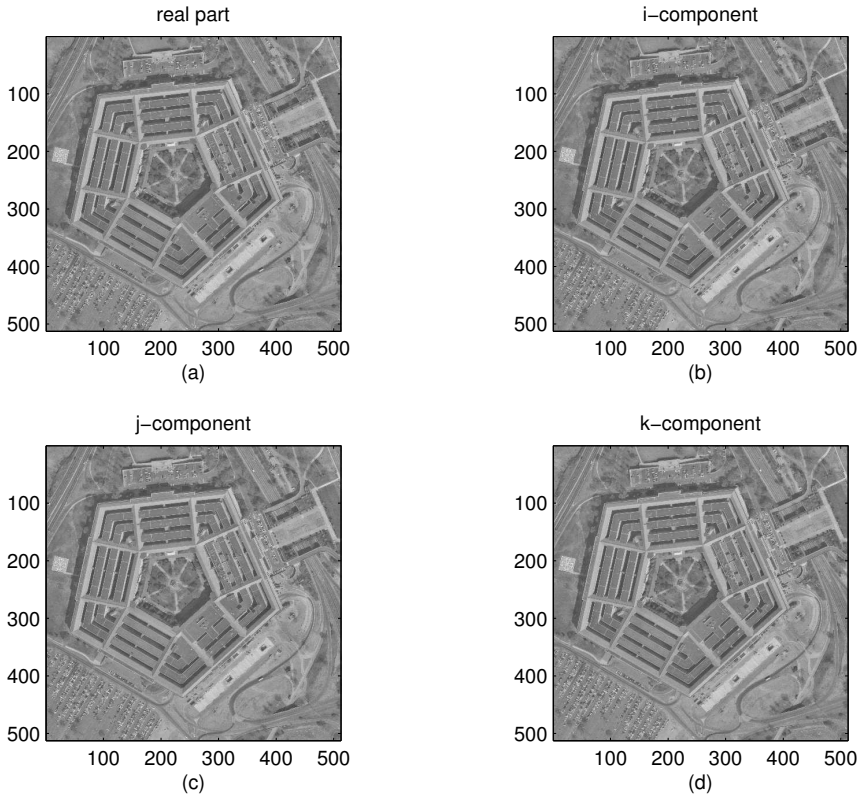


Figure 3. The division of the gray-scale image into four parts of size $512 \times 512$ each. (a) The real part and (b) the $i$-component, (c) the $j$-component, and (d) the $k$-component of the quaternion image.

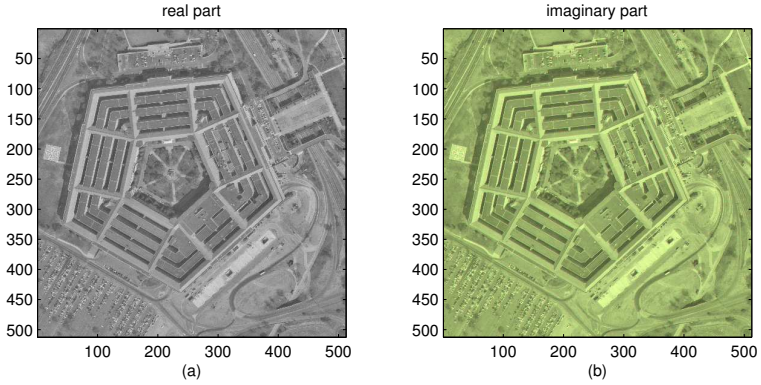


Figure 4. The quaternion image of size $512 \times 512$: (a) the real part and (b) the imaginary part in the RGB color model.

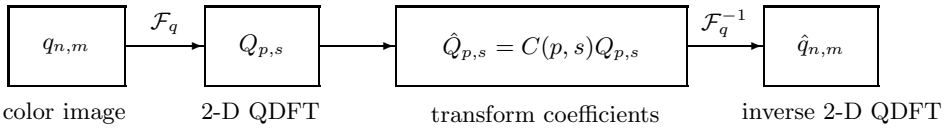


Figure 5. General block-diagram of the quaternion Fourier transform-based image enhancement.

parameter $\alpha$ can also be considered as a function which takes different values on different frequency bands.[29,30] The frequency bands separated by circles are effective when processing the image by the 2-D quaternion Fourier transform. Together with the alpha-rooting, other transform-based image enhancement methods, including the weighted $\alpha$-rooting, modified unsharp masking, and filtering also can effectively be used in image enhancement.[13]

The measure of quality of images can be used for selecting processing parameters for image enhancement. We consider the quantitative measure EME of image enhancement described in[27-29] To measure the quality of images and to select optimal (or best) processing parameters for image enhancement, we can use two different approaches.

1. We consider the known enhancement measure of image processing, $f_{n,m} \to \hat{f}_{n,m}$, which is calculated by

$$EME_a(\hat{f}) = \frac{1}{k_1 k_2} \sum_{k=1}^{k_1} \sum_{l=1}^{k_2} 20 \log_{10} \left[ \frac{\max_{k,l}(\hat{f})}{\min_{k,l}(\hat{f})} \right]. \tag{1}$$

Here, the discrete image $\{f_{n,m}\}$ of size $N \times M$ is divided by $k_1 k_2$ blocks of size $L_1 \times L_2$ where integers $k_1 = \lfloor N/L_i \rfloor$ and $k_2 = \lfloor M/L_2 \rfloor$, where $\lfloor . \rfloor$ denotes the floor function. $\max_{k,l}(\hat{f})$ and $\min_{k,l}(\hat{f})$ respectively are the maximum and minimum of the image $\hat{f}_{n,m}$ inside the $(k,l)$th block, and $a$ is a parameter, or a vector parameter, of the enhancement algorithm. We call $a_0$ such that $EME_{a_0}(\hat{f}) = \max EME_a(\hat{f})$ the best (or optimal) Fourier transform-based image enhancement parameter[13,21,26-30]

Example 1. We consider the 1024 "pentagon" image. Figure 6 shows this image in part (a), and the enhancement by the 0.89-rooting by the 2-D DFT in part (b). The enhancement measure for the original image is 9.3487, and 27.6140 for the enhanced image in (b). The graph of the EME measure of the $\alpha$-rooting, as the function of

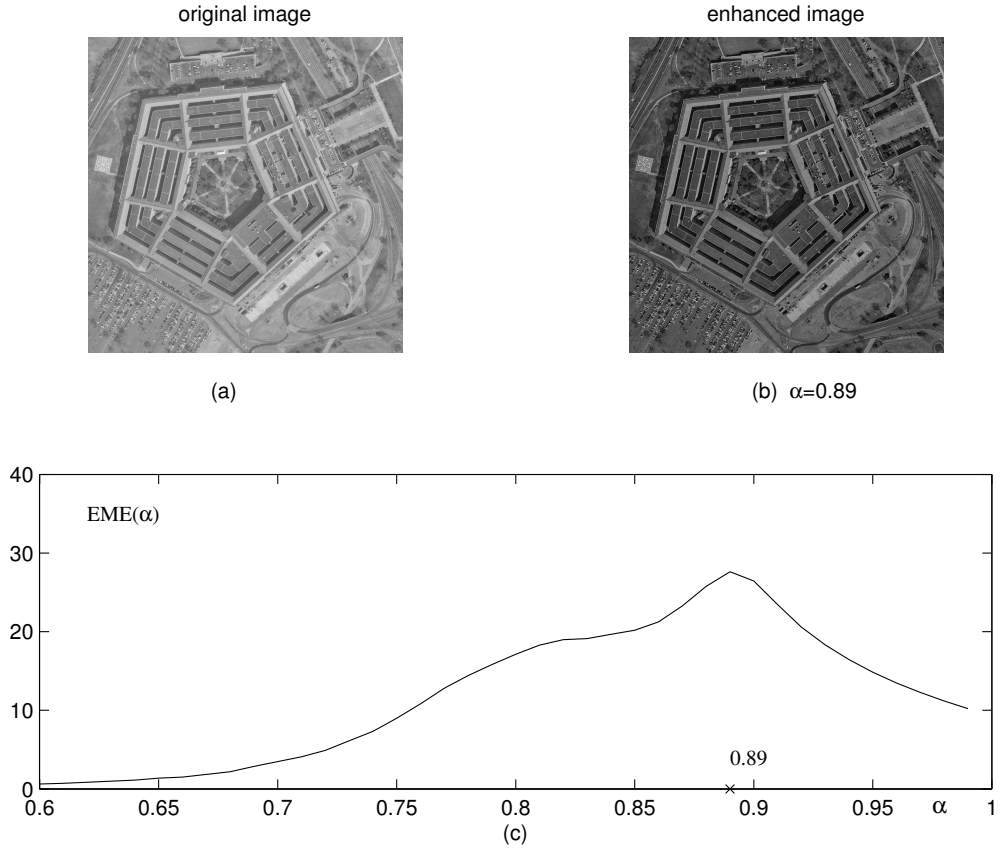


Figure 6. (a) The "pentagon" image, (b) the image enhanced by the 0.89-rooting, and (c) the EME measure of the $\alpha$-rooting by the 2-D DFT.

$\alpha$ in shown in part c. This function has the maximum at point 0.89.

2. In quaternion images, including color images, EME measure can be calculated separately for each color component. Figure 7 shows the color image or component of the quaternion "pentagon" image in part (b),

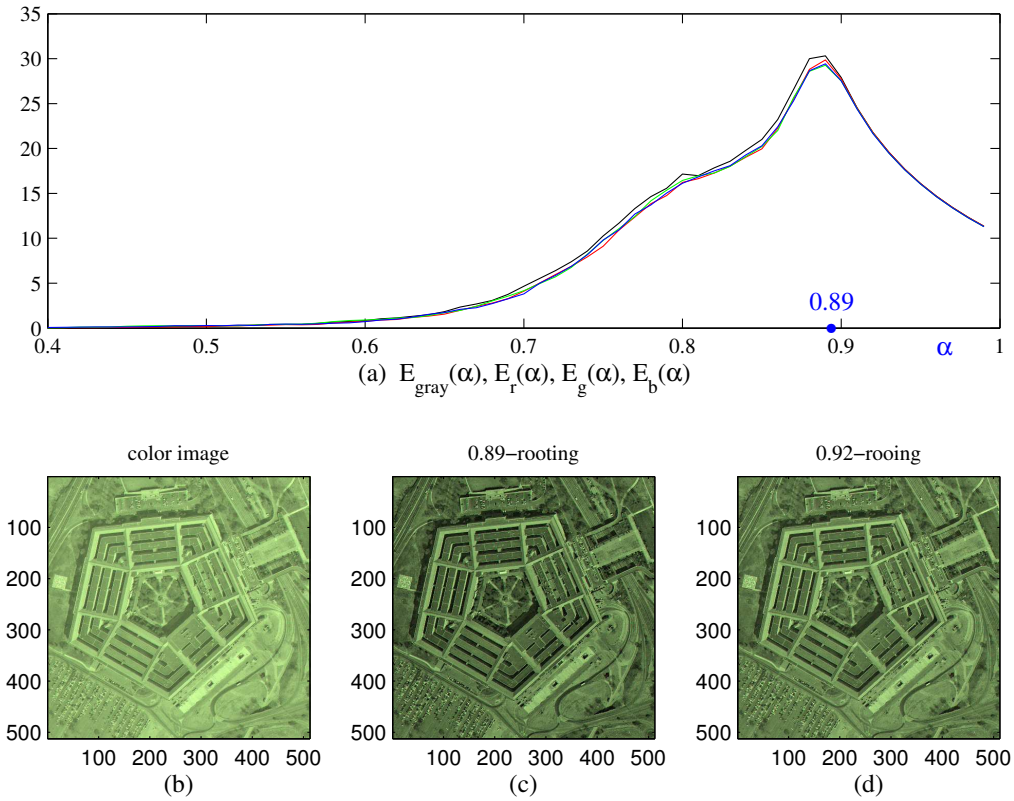


Figure 7. (a) Four EME measures of the ($\alpha$-rooting by the 2-D DFT, and the imaginary parts of (b) the quaternion "pentagon" image, and the images enhanced by (c) the 0.89-rooting and (d) the 0.92-rooting.

and the results of the 0.89-rooting and 0.92-rooting in parts (c) and (d), respectively. The enhancement was performed by using the 2-D right-side QDFT. The parameter 0.89 was selected by analyzing the graphs EME measures for components of the quaternion image, which are shown in part (a).

However, instead of calculating the functions $EME_a(\hat{f}_R)$, $EME_a(\hat{f}_G)$, and $EME_a(\hat{f}_B)$, the following enhancement measure of the color image $\hat{f} = (\hat{f}_R, \hat{f}_G, \hat{f}_B)$, which we call EMEC,[1,2,20,26] can be calculated:

$$EMEC(\hat{f}) = \frac{1}{k_1 k_2} \sum_{k=1}^{k_1} \sum_{l=1}^{k_2} 20 \log_{10} \left[ \frac{\max_{k,l}\{\hat{f}_R, \hat{f}_G, \hat{f}_B\}}{\min_{k,l}\{\hat{f}_R, \hat{f}_G, \hat{f}_B\}} \right]. \tag{2}$$

The images are in the RGB color space, i.e., $f = (f_R, f_G, f_B)$ and $\hat{f} = (\hat{f}_R, \hat{f}_G, \hat{f}_B)$. The maximum and minimum values of the image $\hat{f}$ in the $(k,l)$-th block are calculated as $\max(\hat{f}) = \max(\hat{f}_R, \hat{f}_G, \hat{f}_B)$ and $\min(\hat{f}) = \min(\hat{f}_R, \hat{f}_G, \hat{f}_B)$. Thus, one EMEC measure can be used instead of four EME.

As an example, Figure 8 shows the EMEC measure of image enhancement by the method of $\alpha$-rooting over the quaternion "pentagon" image. The maximum of this function $E_q(\alpha) = EMEC(\alpha)$ is at the same point 0.89.

Figure 9 shows the original "pentagon" image in part (a) together with the result of enhancement by the 0.89-rooting in quaternion space in part (b).

Example 2. The gray-scale image of size $1024 \times 1024$, which we call the "airport" image, is shown in part (a) of Figure 10. The real of this image after transforming to the quaternion space is shown in part (b), and the imaginary part as a color image is shown in part (c).

Figure 11 shows the graphs of all four image enhancement measures of alpha-rooting by the 2-D QDFT in part (a). The maximum of these functions at the point $\alpha = 0.92$. The imaginary part of the original quaternion

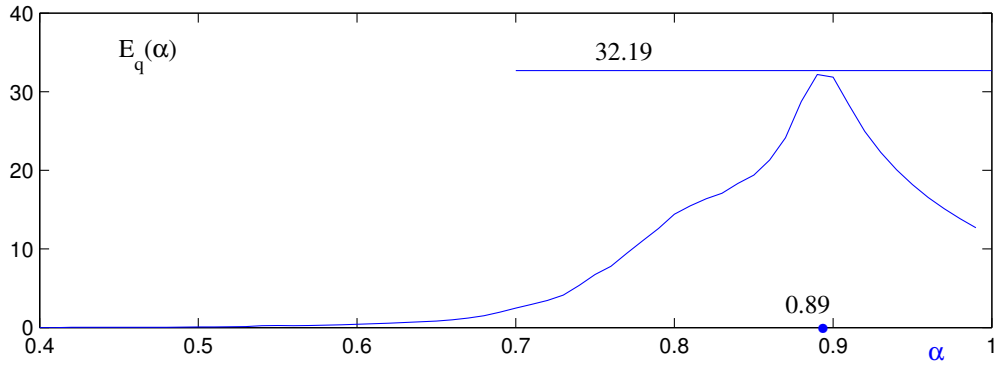


Figure 8. The EMEC measure of the $\alpha$-rooting by the 2-D QDFT.

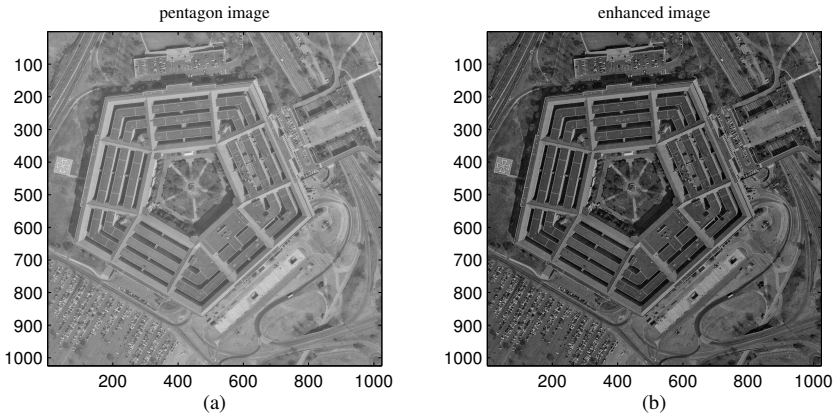


Figure 9. (a) The original gray-scale "pentagon" image of size $1024 \times 1024$ and (b) the enhanced image

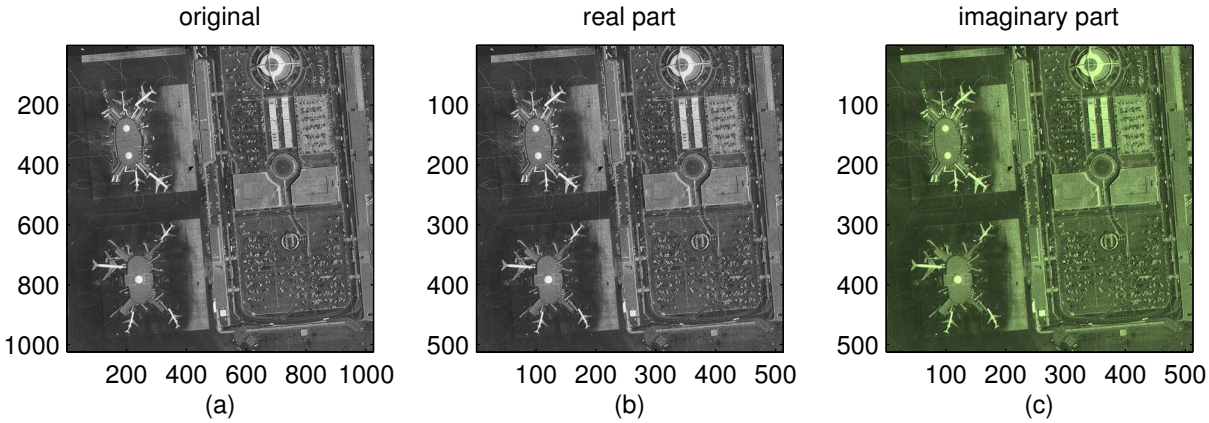


Figure 10. (a) The original gray-scale "5.3.02" image of size $1024 \times 1024$ and (b) the real part and (c) the imaginary (color) part of the image in the quaternion space.

image as the color image is shown in part (b). The corresponding color images of the 0.92-rooting and the 0.96-rooting are shown in parts (c) and (d), respectively.

Figure 9 shows the EMEC measure of image enhancement by the method of $\alpha$-rooting over the quaternion image.

The result of funding the best alpha parameter, when using one enhancement measure EMEC is shown in Figure 8. The EMEC graph of is shown in part (a), the original gray-scale "airport" image in part (b), and the

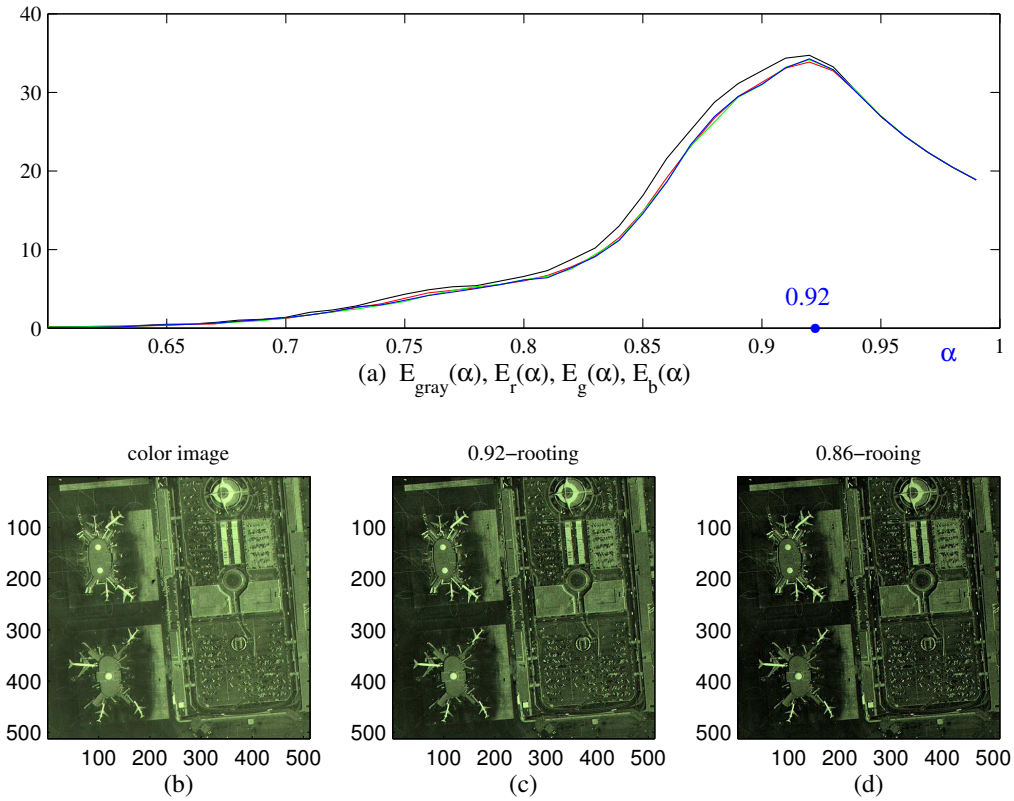


Figure 11. (a) Four EME measures of the $\alpha$-rooting by the 2-D QDFT, and the imaginary parts of (b) the quaternion "pentagon" image, and the images enhanced by (c) the 0.89-rooting and (d) the 0.92-rooting.

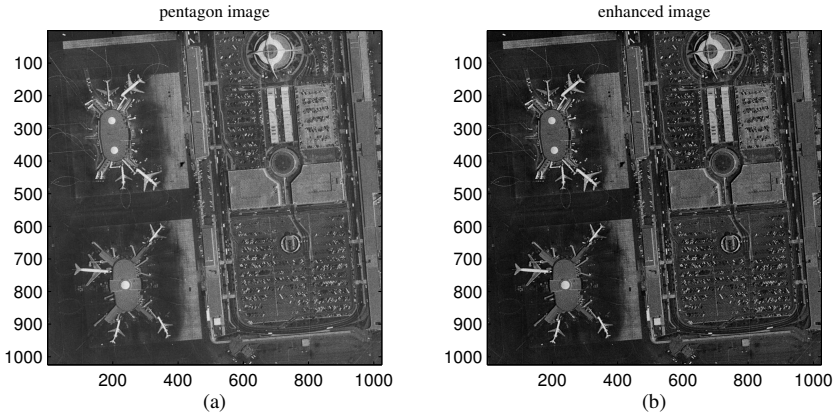


Figure 12. (a) The original gray-scale "airport" image of size $1024 \times 1024$ and (b) the enhanced image after processing by the $\alpha$-rooting in the quaternion space.

enhanced image by the proposed method in the quaternion space in part (c).

## 6. THE RIGHT-SIDE 2-D QDFT

In this section, we consider the concept of the right-side 2-D QDFT, which was used for image enhancement in the frequency domain. This transform can be effectively calculated not only by the row-column method, but with the concept of the tensor and paired representations[1,19,26]-.[30] The concept of the left-side 2-D QDFTs[6]-[8] can be described similarly. Such representation allow for reducing the calculation of the 2-D QDFTs to the calculation

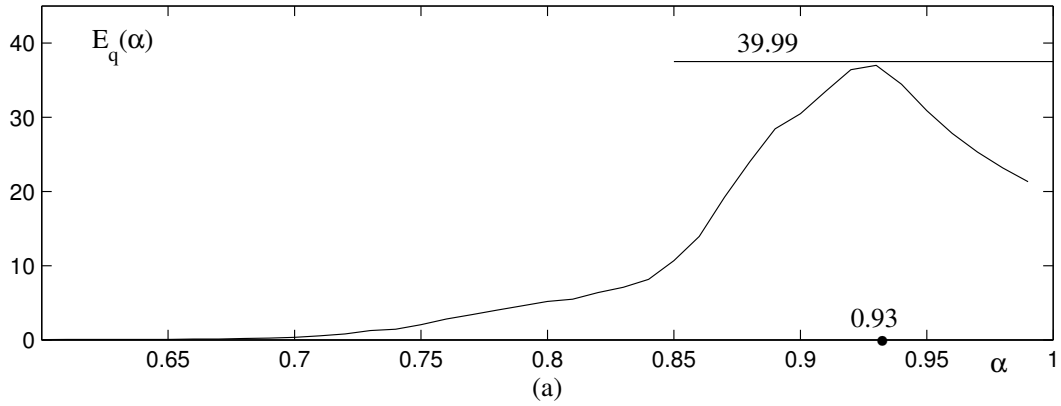


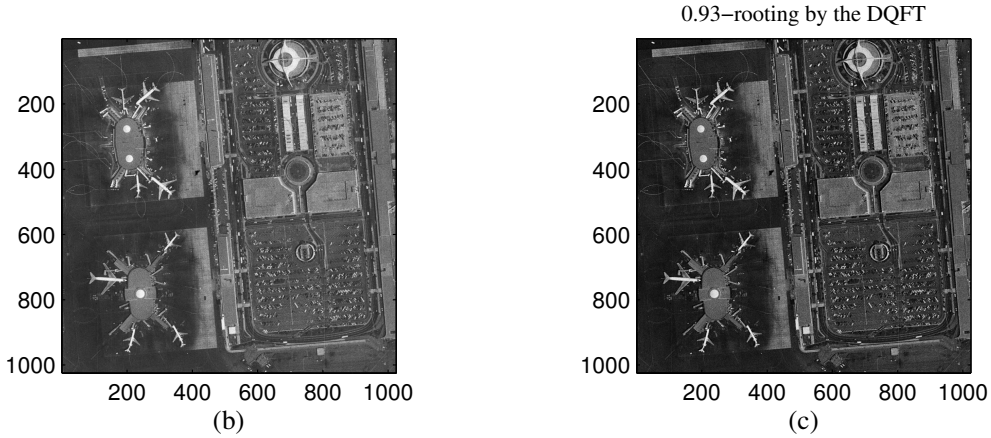


Figure 13. (a) The EMEC measure of the $\alpha$-rooting by the 2-D QDFT, (b) the original "airport" image, and (c) the enhanced image by the 0.92-rooting in the quaternion space.

of the 1-D QDFTs over the splitting-signals which represent the image and can be used for image processing.[20,25] Therefore, the calculation of the 2-D QDFT as well as 2-D ODFT can be reduced to separate calculation of the 1-D transforms, and application of transforms in color image enhancement,[17,18,30] filtration[13,21,31] and image reconstruction[32]-.[40]

Let $q_{n,m}$ be the quaternion discrete image of size $N \times N$, and let $\mu$ be the pure unit quaternion, $\mu^2 = -1$. The right-side 2-D QDFT as a generalized quaternion Fourier transform is defined as

$$Q_{p,s} = \sum_{n=0}^{N-1} \sum_{m=0}^{N-1} q_{n,m} W_\mu^{np+ms}, \quad p, s = 0 : (N-1). \tag{3}$$

The kernel of the right-side 2-D QDFT is defined by the exponential function $W_\mu = W_{\mu;N} = \exp(-2\pi\mu/N)$. Here, the equality $W_\mu^{np} = (W_\mu)^{np} = \exp(-\mu 2\pi np/N)$ holds. The inverse right-side 2-D QDFT is calculated by

$$q_{n,m} = \frac{1}{N^2} \sum_{p=0}^{N-1} \sum_{s=0}^{N-1} Q_{p,s} W_\mu^{-(np+ms)}, \quad n, m = 0 : (N-1).$$

As an example, Figure 14 shows the real part of the 2-D QDFT of the quaternion "pentagon" image in part (a),

$$Q_{p,s} = (Q_{p,s})_e + \Big(i(Q_{p,s})_i + j(Q_{p,s})_j + k(Q_{p,s})_k\Big), \quad p, s = 0 : 511,$$

in the absolute scale. The imaginary part of the transform is shown in parts (b) and (c). One can see, that the real part of the 2-D QDFT is not a dominant component in the quaternion spectrum of the image.

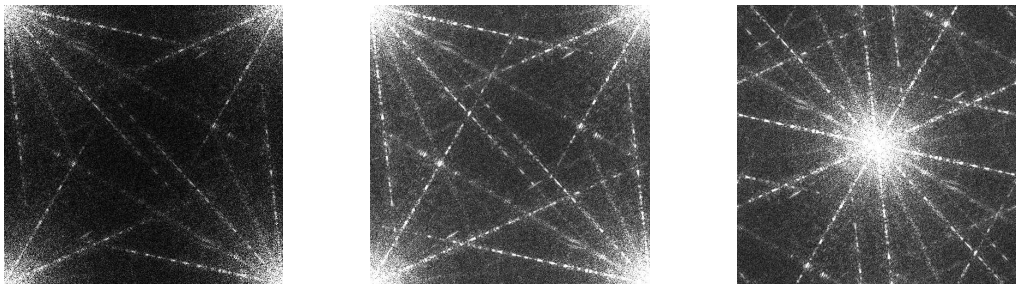

(a) (b) (c)

Figure 14. The magnitudes of (a) real component, $|Q_{p,s})_e|$, and imaginary component, $\sqrt{(Q_{p,s})_i^2 + (Q_{p,s})_j^2 + (Q_{p,s})_k^2}$, before (b) and after (c) cyclicly shifting to the center.

## 7. CONCLUSION

New approach of image enhancement is proposed for gray-scale images, which is based on the idea of transforming the image into the quaternion space, where the image can be enhanced and filtered by using the concept of the two-dimension quaternion discrete Fourier transform (2-D QDFT). The application of the proposed method is described on the example of alpha-rooting. Our preliminary results show that the application of the 2-D QDFT plus the alpha-rooting method can be effectively used for enhancing gray-scale images.

## REFERENCES


[1] A.M. Grigoryan and S.S. Agaian, *Practical Quaternion Imaging with MATLAB,* SPIE Press, 2017.

[2] A.M. Grigoryan and S.S. Agaian, "Retolling of color imaging in the quaternion algebra," *Applied Mathematics and Sciences: An International Journal (MathSJ),* vol. 1, no. 3, pp. 23-39, 2014.

[3] S.J. Sangwine, "Fourier transforms of colour images using quaternion, or hypercomplex, numbers," *Electronics Letters,* vol. 32, no. 21, pp. 1979–1980, 1996.

[4] S.J. Sangwine, T.A. Ell, "Hypercomplex Fourier transforms of color images," in Proc. *IEEE Intl. Conf. Image Process.,* vol. 1, pp. 137-140, 2001.

[5] T.A. Ell, "Quaternion-Fourier transforms for analysis of 2-dimensional linear time-invariant partial differential systems," In Proc. of the 3nd *IEEE Conference on Decision and Control,* vol. 1-4, December 1993, pp. 1830–1841, San Antonio, Texas, USA.

[6] A.M. Grigoryan, S.S. Agaian, "Tensor transform-based quaternion Fourier transform algorithm," *Information Sciences*, vol. 320, pp. 62-74, November 2015, (doi: http://dx.doi.org/10.1016/j.ins.2015.05.018)

[7] A.M. Grigoryan, S.S. Agaian, "2-D Left-side quaternion discrete Fourier transform fast algorithms," *Proceedings of IS&T International Symposium, 2016 Electronic Imaging: Algorithms and Systems XIV,* San Francisco, California, February 2016.

[8] A.M. Grigoryan, S.S. Again, "Tensor representation of color images and fast 2-D quaternion discrete Fourier transform," [9399-16], *Proceedings of SPIE,* vol. 9399, 2015 Electronic Imaging: Image Processing: Algorithms and Systems XIII, San Francisco, California, February 2015.

[9] W.R. Hamilton, *Lectures on quaternions: Containing a systematic statement of a new mathematical method,* Dublin: Hodges and Smith (1853).

[10] W.R. Hamilton, *Elements of Quaternions,* Logmans, Green and Co., London, 1866.

[11] L. Rabiner, B. Gold, *Theory and application of digital signal processing,* Prentice-Hall Inc., 1975.

[12] S.S. Agaian, "Advances and problems of the fast orthogonal transforms for signal-images processing applications (Part 1)," in: *Pattern Recognition, Classification, Forecasting. Yearbook, The Russian Academy of Sciences, Nauka,* Moscow, Issue 3, pp. 146-215, 1990.

[13] A.M. Grigoryan, S.S. Agaian, *Multidimensional discrete unitary transforms: Representation, partitioning and algorithms,* Marcel Dekker Inc., New York, 2003.

[14] A.M. Grigoryan, S.S. Agaian, "Split manageable efficient algorithm for Fourier and Hadamard transforms, *IEEE Trans. Signal Processing,* vol. 48, no. 1, pp. 172-183, 2000.

[15] Z. Yang and S.-I. Kamata, "Hypercomplex polar Fourier analysis for color image," Proceedings - International Conference on Image Processing, ICIP 2011.

[16] A. Greenblatt, C.M. Lopez, Sos S. Agaian, "Quaternion neural networks applied to prostate cancer Gleason grading, in Proceedings, Man and Cybernetics, SMC 2013. IEEE International Conference, Manchester, pp. 1144–1149, 2013.

[17] A.M. Grigoryan and S.S. Agaian, "Cell Phone Camera Color Medical Imaging via Fast Fourier Transform," chapter 3, pp. 33–76, in book Mobile Imaging for Healthcare Applications, (J. Tang, S. Agaian, and J. Tan, Editors), *SPIE Press,* January 2016.
[18] A.M. Grigoryan and S.S. Agaian, "Color Enhancement and Correction for Camera Cell Phone Medical Images Using Quaternion Tools," chapter 4, pp. 77–117, in book Mobile Imaging for Healthcare Applications, (J. Tang, S. Agaian, and J. Tan, Editors), *SPIE Press,* January 2016.
[19] S.C. Pei, J.J. Ding, and J.H. Chang, "Efficient implementation of quaternion Fourier transform, convolution and correlation by 2-D complex FFT," IEEE Trans. Signal Process., vol. 49, pp. 2783-2797, 2001.
[20] A.M. Grigoryan, J. Jenkinson, S.S. Agaian, "Quaternion Fourier transform based alpha-rooting method for color image measurement and enhancement," *SIGPRO-D-14-01083R1, Signal Processing,* vol. 109, pp. 269–289, April 2015, (doi:10.1016/j.sigpro.2014.11.019)
[21] A.M. Grigoryan and M.M. Grigoryan, *Brief Notes in Advanced DSP: Fourier Analysis With MATLAB.,* CRC Press Taylor and Francis Group, 2009.
[22] A.M. Grigoryan, "2-D and 1-D multi-paired transforms: Frequency-time type wavelets," *IEEE Trans. on Signal Processing,* vol. 49, no. 2, pp. 344–353, Feb. 2001.
[23] A.M. Grigoryan, "Fourier transform representation by frequency-time wavelets," *IEEE Trans. on Signal Processing,* vol. 53, no. 7, pp. 2489-2497, July 2005.
[24] A.M. Grigoryan, "Multidimensional Discrete Unitary Transforms," chapter 19 (69 pages), in Third Edition Transforms and Applications Handbook in The Electrical Engineering Handbook Series (Editor in Chief, Prof. Alexander Poularikas), *CRC Press, Taylor and Francis Group,* January 11, 2010.
[25] A.M. Grigoryan, K. Naghdali, "On a method of paired representation: Enhancement and decomposition by series direction images," *Journal of Mathematical Imaging and Vision,* vol. 34, no. 2, pp. 185–199, June 2009.
[26] A.M. Grigoryan, S.S. Agaian, "Alpha-rooting method of color image enhancement by discrete quaternion Fourier transform," [9019-3], in Proc. *SPIE 9019, Image Processing: Algorithms and Systems XII,* 901904 (25 February 2014); 12 p., doi: 10.1117/12.2040596
[27] S.S. Agaian, K. Panetta, A.M. Grigoryan, "A new measure of image enhancement," in Proc. of the IASTED International Conference on Signal Processing & Communication, Marbella, Spain, Sep. 19-22, 2000.
[28] S.S. Agaian, K. Panetta, A.M. Grigoryan, "Transform-based image enhancement algorithms," *IEEE Trans. on Image Processing,* vol. 10, no. 3, pp. 367–382, 2001.
[29] A.M. Grigoryan, S.S. Agaian, "Transform-based image enhancement algorithms with performance measure," *Advances in Imaging and Electron Physics, Academic Press,* vol. 130, pp. 165–242, 2004.
[30] F.T. Arslan, A.M. Grigoryan, "Fast splitting $\alpha$-rooting method of image enhancement: Tensor representation," *IEEE Trans. on Image Processing,* vol. 15, no. 11, pp. 3375–3384, Nov. 2006.
[31] A.M. Grigoryan, E.R. Dougherty, S.S. Agaian, "Optimal Wiener and Homomorphic Filtration: Review," *Signal Processing,* vol. 121, pp. 111–138, April 2016, (doi:10.1016/j.sigpro.2015.11.006)
[32] A.M. Grigoryan, "Solution of the problem on image reconstruction in computed tomography," *Journal of Mathematical Imaging and Vision,* vol. 54, Issue 1, pp. 35–63, January 2016. (doi: 10.1007/s10851-015-0588-6)
[33] A.M. Grigoryan, M.M. Grigoryan, *Image processing: Tensor transform and discrete tomography with MATLAB,* CRC Press Taylor and Francis Group, 2012.
[34] A.M. Grigoryan, "Method of paired transforms for reconstruction of images from projections: Discrete model," *IEEE Transactions on Image Processing,* vol. 12, no. 9, pp. 985-994, September 2003.
[35] A. Grigoryan, S. Agaian, "Tensor form of image representation: enhancement by image-signals," in Proc. *IS&T/SPIEs Symposium on Electronic Imaging Science & Technology,* San Jose. CA, 22-23 January 2003.
[36] A.M. Grigoryan and N. Du, "Novel tensor transform-based method of image reconstruction from limited-angle projection data," [9020-14], *SPIE proceedings, 2014 Electronic Imaging: Computational Imaging XII,* February 2-6, San Francisco, California, 2014.
[37] A.M. Grigoryan, Nan Du, "2-D images in frequency-time representation: Direction images and resolution map," *Journal of Electronic Imaging,* vol. 19, no. 3 (033012), July-September 2010.
[38] A.M. Grigoryan and Nan Du, "Principle of superposition by direction images," *IEEE Trans. on Image Processing,* vol. 20, no. 9, pp. 2531–2541, September 2011.
[39] A.M. Grigoryan, "Image reconstruction from finite number of projections: Method of transferring geometry," *IEEE Trans. on Image Processing,* vol. 22, no. 12, pp. 4738–4751, December 2013.
[40] A.M. Grigoryan, "Another Step towards Successful Tomographic Imaging in Cancer: Solving the Problem of Image Reconstruction," in book Computer-Aided Cancer Detection and Diagnosis: Recent Advances" (J. Tang and S. Agaian, Editors), *SPIE Press,* chapter 11, pp. 295–338, January 2014.